LARGE-EDDY SIMULATION OF THE FLOW AROUND A HIGH-LIFT AIRFOIL CONFIGURATION

Daniel König[†], Wolfgang Schröder, Matthias Meinke
Institute of Aerodynamics,
RWTH Aachen University
Wüllnerstraße zw. 5 und 7, 52062 Aachen, Germany
[†]d.koenig@aia.rwth-aachen.de

ABSTRACT

To identify the flow phenomena generating slat noise, a large-eddy simulation (LES) of the flow around an airfoil consisting of a slat and a main wing is performed at a Reynolds number of 1.4 million based on the freestream velocity and the clean chord length. The freestream Mach number is $Ma = 0.16$ and the angle of attack is 13° deg. Sponge layers are used to avoid spurious reflections at the outer boundaries of the computational domain. A computational mesh with about 55 million cells are used to resolve the turbulent scales in the boundary layers and within the slat cove region. The comparison with experimental data shows acceptable agreement for the pressure and Mach number distribution. The detailed analysis of the external flow field reveals boundary layer transition. The turbulent structures of the slat cove shear layer are compared to those in a plane shear layer. The shear layer behavior in the reattachment region is assessed by the mechanisms of an impinging jet. It is shown that the major acoustic source, the perturbed Lamb vector, coincides with areas of high turbulent kinetic energy.

INTRODUCTION

The magnitude of the emitted airframe noise will be an important factor in the future development process of aircraft due to the continuously increasing air traffic and the stricter licensing requirements. Since tremendous progress has been made in reducing jet noise it is airframe noise that is more or less equally important. Especially during the landing approach, when the engines run almost in idle condition, the airframe noise is the dominant part of the emitted sound. The main contributions are from landing gears and the wing, where especially high-lift devices, i.e., slats and flaps, represent major noise sources. The development of low-noise aircraft demands on the one hand, an investigation of the sound generating mechanisms, which on the other hand, require a detailed knowledge of the underlying turbulent flow field. For this purpose, a large-eddy simulation of a high-lift airfoil configuration consisting of a slat and a main wing is conducted to meticulously analyze the flow field in the slat area.

NUMERICAL METHOD

The three-dimensional unsteady compressible Navier-Stokes equations are solved based on a large-eddy simulation (LES) formulation using the MILES (monotone integrated LES) approach (Boris et al. 1992). The vertex-centered finite-volume flow solver is block-structured. This discretization is based on a modified AUSM method for the inviscid terms (Liou and Steffen 1993) with second-order accuracy. For the viscous terms a centered approximation of second-order is used. The temporal integration from time level n to $n+1$ is done by a second-order accurate explicit 5-stage-Runge-Kutta method, the coefficients of which are optimized for maximum stability. For a detailed description of the flow solver the reader is referred to Meinke et al. (2002). For low Mach number flows a preconditioning method in conjunction with a dual-time stepping scheme can be used (Alkishriwi et al. 2006). Furthermore, a multi-grid method is implemented to accelerate the convergence within the artificial time.

COMPUTATIONAL SETUP

The computational mesh used for the LES consists of 32 blocks with a total number of 55 million grid points. The extent in the spanwise direction amounts to 2.1% of the clean chord length and is resolved by 65 points. Figure 1 shows the computational grid in the slat cove region. Using the friction velocity $u_* = \sqrt{\tau_w/\rho}$ to define the non-dimensional inner coordinates $\Delta h_i^+ = \Delta h u_*/\nu$ the mesh resolution near the surface was $\Delta x^+ \approx 100$, $\Delta y^+ \approx 1$, and $\Delta z^+ \approx 22$. These values were approximated by the analytical solution of a flat plate during the grid generation process.
On the far-field boundaries of the computational domain boundary conditions based on the theory of characteristics are applied. A sponge layer following Israeli and Orszag (1981) is imposed on these boundaries to avoid spurious reflections, which would harm future acoustic analyses. On the walls, an adiabatic no-slip boundary condition is applied with a zero pressure gradient normal to the wall. In the spanwise direction periodic boundary conditions are used.
The computation is performed for a freestream Mach number of $Ma = 0.16$ at an angle of attack of 13°. The Reynolds number, which is based on the clean chord length and the freestream velocity, amounts to 1.4 million. These parameters correspond to experiments conducted in the AWB wind tunnel at DLR Braunschweig within the research project FREQUENZ.
To initialize the flow field a two-dimensional compressible RANS solution was provided.

RESULTS

The discussion of the results starts with some general information about the computation and data sampling. Then, the grid quality of the mesh is assessed. Next, we analyze the mean flow structure and compare numerical and experimental findings. Subsequently, a discussion of the instantaneous turbulent flow structures follows. Finally, we investigate the structure of the major noise source, i.e., the distribution of the Lamb vector.

The simulation was run for about 5 non-dimensional time units based on the freestream velocity and the clean chord length until a fully developed turbulent flow field was obtained. Subsequently, samples were collected at a time interval of approximately 0.0015 time units for the statistical analyses and also to compute the source terms for the aeroacoustic analyses. In total about 3500 data sets were recorded covering an overall time of about 5 time units and requiring 7 Terabytes of disk space.

First, the quality of the obtained results is assessed by the grid resolution near the walls. Since the slat cove flow is of primary interest in this analysis only the resolution values of this area are shown in Fig. 2. All other near wall regions have equally good resolutions. Based on the analysis of Sagaut (2003) it is evident that the required values $\Delta x^+ \approx 100$, $\Delta y^+ \approx 1$, and $\Delta z^+ \approx 22$ for a sufficient near-wall resolution in an LES are reached on almost all surfaces.

In Fig. 3 the pressure coefficient c_p of the time and spanwise averaged flow field is compared with a RANS solution based on a one-equation turbulence model (Fares and Schröder 2004) and experimental data (Kolb 2006). The measurements were conducted in an anechoic wind tunnel with an open test section. The experimental results are compared with numerical solutions, which mimic uniform freestream conditions. Therefore, even by correcting the geometric angle of attack of 23° in the measurements to 13° in the numerical solution no perfect match between the experimental and numerical data can be expected. The necessary correction of the angle was determined by RANS simulations, which explains the good agreement of the experimental findings with the RANS results.

The Mach number distribution and some selected streamlines of the time and spanwise averaged flow field are depicted in Fig. 4. Two stagnation points are visible, one near the nose of the slat and the other one on the lower side of the main airfoil. It is evident that the slat cove region is an area of very low Mach number, which is characterized by a strong recirculation being illustrated by the streamlines. This recirculation area is separated from the flow passing the slat gap by a shear layer, which emanates at the slat cusp. Furthermore, shortly downstream of the slat gap the highest Mach numbers occur. In Fig. 5 the result from a particle-image velocity (PIV) measurement is shown (Abstiens 2007). The laser for the light section was positioned beneath the high-lift configuration such that no data for the flow on the suction side is available. However, it is obvious that the computational and experimental findings on the pressure side are in very good agreement. The confusing distribution between the slat cusp and the main wing stagnation point is caused by some diffuse reflections due to the test arrangement. Figures 6 to 8 show the LES and experimental velocity distribution on the lines A, B, and C, as a function of the non-dimensional coordinate s. Their locations are defined in Fig. 4. Except for the near wall regions, where slight differences are visible, the numerical and experimental results are in very good agreement. Figure 8 shows that both, the large-eddy simulation and the PIV measurement, determine approximately likewise recirculation zones in the slat cove.

The distribution of the turbulent kinetic energy $k = \frac{1}{2}\left(u'^2 + v'^2 + w'^2\right)$ is depicted in Fig. 9. High k values occur in the shear layer, the recirculation area, and in the wake of the slat trailing edge. The major magnitudes of k are produced by the reattaching shear layer where the flow is decomposed. This is in good agreement with the results presented by Choudhari and Khorrami (2006).

In the following, we will have a closer look at the unsteady turbulent structures in the slat region. The visualization of the vortical structures is done by λ_2 contours following the work of Jeong and Hussain (1995). Figure 10 reveals areas of turbulent flow to be located in the boundary layers of the slat and main airfoil, downstream of the slat trailing edge, and in the slat cove region. The transition of the boundary layer from laminar to turbulent flow occurs shortly downstream of the leading edges and without incorporating any special perturbations.

The turbulent flow in the slat cove is bounded by a turbulent shear layer which develops from the slat cusp and reattaches near the slat trailing edge. Figure 11 depicts the vortical structures in the shear layer and the slat cove. The greyscales mapped onto the λ_2 contours visualize the Mach number distribution. The structures in the slat cove rotate in a counter-clockwise direction around the center of the recirculation area. The predominant size of the structures shortly before they reach the slat cusp is small compared to the remainder of the slat cove areas. It is obvious, this region is distinguished by a strong deflection of the flow which is caused by the geometry.

The shear layer starts to behave as expected with the formation of predominantly two-dimensional, spanwise vortex structures in the following referred to as rollers which are a result of the velocity profile in the shear layer and the associated Kelvin-Helmholtz instability (Rogers and Moser 1992). Figure 12 shows the λ_2 contours in the near slat cusp region, where the early rollers occur. Furthermore, the vortical structures from the slat cove recirculation area penetrate into the shear layer and distort the rollers. This mixing and interaction of shear layer structures with structures from the recirculation area seem to lead to instabilities, which enhance the development of streamwise orientated vortical structures between two rollers. Similar structures, which are termed rib vortices, have been described e.g. by Rogers and Moser (1992) and Sakakibara et al. (2001). Figure 14 shows some rollers and rib vortices shortly before the shear layer enters the reattachment area. Also note the sinusoidal appearance of the rollers. It seems that the rollers develop a slightly curved or wavy shape, respectively, due to their interaction with the rib vortices.

The vortical structures of the shear layer in the reattachment area are compared to those of a plane impinging jet. One great difference between the slat generated shear layer and the plane jet is the missing symmetry. However, for a first analysis of the vortical structures in the reattachment region the plane impinging jet seems to be appropriate. Figure 15 illustrates some more pronounced vortices being generated in the reattachment region. Their axes are aligned with the steamwise direction. Similar vortical structures have been observed by Sakakibara et al. (2001), who called them wall ribs. In the case of the jet the wall ribs are formed by the impinging successive and cross ribs. In the present shear layer no cross ribs occur due to the missing symmetry, which is required for their development (Sakakibara et al. 2001). However, it can be seen that the successive ribs correspond to the streamwise ribs of the present solution. Unlike the jet rollers the shear layer rollers have a contribution to the wall ribs. This is due to the sinusoidal rollers in the spanwise direction and the acceleration of the flow passing through the slat gap. It is obvious that the parts of the rollers pointing in the direction of the slat gap undergo a stronger acceleration leading to a pronounced distortion of the rollers such that they finally collapse. The remaining structures are predominantly aligned with the streamwise direction. This explains

the periodically changing strength and location of the wall ribs. The wall ribs, which are captured in the recirculation area, are decomposed very fast by the high influence of the rotating flow. An closer look at the position of the reattachment point reveals a slight forward and backward motion, which is in agreement with findings of Choudhari and Khorrami (2006).
Figure 13 shows at the slat trailing edge a turbulent wake to develop. This wake consists of the structures of the turbulent boundary layer on the suction side of the slat and the vortical structures, which are convected through the slat gap and which are generated in the slat cove area. Unlike the flow downstream of the slat cusp no rollers develop. This is a result of the minimum thickness of the trailing edge of the slat and of the vanishing velocity difference across the wake, which is due to the highly accelerated flow through the slat gap. The wall ribs generated in the reattachment region are conserved for quite some distance until they dissolve due to the influence of a slight adverse pressure gradient.
Finally, we show the distribution of the major source term for further acoustic analyses, which are based on the acoustic perturbation equations (APE) from Ewert and Schröder (2003). In the case of airframe noise it is sufficient to consider only vortex sound, where the major source is given by the Lamb vector $(\omega \times v)$ (Ewert and Schröder 2004). Figure 16 depicts a snapshot of the norm of the perturbed Lamb vector. It is obvious that the strongest sources occur in the regions with the highest vortical activity and the highest turbulent kinetic energy (Fig. 9), i.e., in the shear layer, the reattachment area, and the slat trailing edge wake.

CONCLUSION

A large-eddy simulation of the turbulent flow over an airfoil in high-lift configuration has been performed. The pressure distribution and the Mach number distribution have been compared with experimental findings. The results show a good agreement. The shear layer, which encloses the turbulent recirculation region in the slat cove, shows turbulent structures comparable to those of a plane mixing layer. In the shear layer reattachment region the generation of wall ribs, which can also be seen in a plane impinging jet, is obvious. The magnitude of the perturbed Lamb vector, which is the major acoustic source for airframe noise, was found coincide to with the areas of highly turbulent flow, i.e., the shear layer, the reattachment area, and the slat trailing edge wake.

ACKNOWLEDGMENT

This work was founded in the framework of the national project FREQUENZ. The computation has been taken place on the SX-8 at the High Performance Computing Center Stuttgart (HLRS). The authors thank Ronald Abstiens and Alexander Kolb for providing the experimental data.

REFERENCES

Abstiens, R. 2007. Private communication. Institute of Aerodynamics, RWTH Aachen University, 2007.

Alkishriwi, N., Schröder, W., and Meinke, M. 2006. A large-eddy simulation method for low mach number flows using preconditioning and multigrid. *Computers and Fluids*, Vol. 35, no. 10, pp. 1126–1136.

Boris, J. P., Grinstein, F. F., Oran, E. S., and Kolbe, R. L. 1992. New insights into large eddy simulation. *Fluid Dynamics Research*, Vol. 10, pp. 199–228.

Choudhari, M. M. and Khorrami, M. R. 2006. Slat cove unsteadiness: Effect of 3d flow structures. In *44st AIAA Aerospace Sciences Meeting and Exhibit*. AIAA Paper 2006-0211.

Ewert, R. and Schröder, W. 2003. Acoustic perturbation equations based on flow decomposition via source filtering. *Journal of Computational Physics*, Vol. 188, pp. 365–398.

Ewert, R. and Schröder, W. 2004. On the simulation of trailing edge noise with a hybrid LES/RANS method. *Journal of Sound and Vibration*, Vol. 270, pp. 509–524.

Fares, E. and Schröder, W. 2004. A general one-equation turbulence model for free shear and wall-bounded flows. *Flow, Turbulence and Combustion*, Vol. 73, pp. 187–215.

Israeli, M. and Orszag, S. A. 1981. Approximation of radiation boundary conditions. *Journal of Computational Physics*, Vol. 41, pp. 115–135.

Jeong, J. and Hussain, F. 1995. On the identification of a vortex. *J. Fluid Mech.*, Vol. 285, pp. 69–94.

Kolb, A. 2006. Private communication. FREQUENZ, 2006.

Liou, M.-S. and Steffen, C. J. 1993. A new flux splitting scheme. *Journal of Computational Physics*, Vol. 107, pp. 23–39.

Meinke, M., Schröder, W., Krause, E., and Rister, Th. 2002. A comparison of second- and sixth-order methods for large-eddy simulations. *Computers and Fluids*, Vol. 31, pp. 695–718.

Rogers, M. M. and Moser, R. D. 1992. The three-dimensional evolution of a plane mixing layer: the kelvin-helmholtz rollup. *Journal of Fluid Mechanics*, Vol. 243, pp. 183–226.

Sagaut, P. 2003. *LESFOIL: Large Eddy Simulation of Flow Around a High Lift Airfoil*, chap. Contribution by ONERA. Springer.

Sakakibara, J., Hishida, K., and Phillips, W. R. C. 2001. On the vortical structure in an plane impinging jet. *Journal of Fluid Mechanics*, Vol. 434, pp. 273–300.

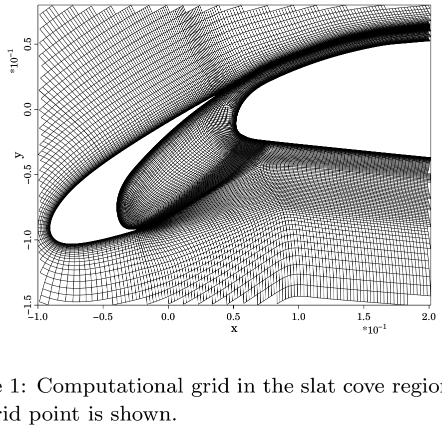

Figure 1: Computational grid in the slat cove region. Every 2nd grid point is shown.

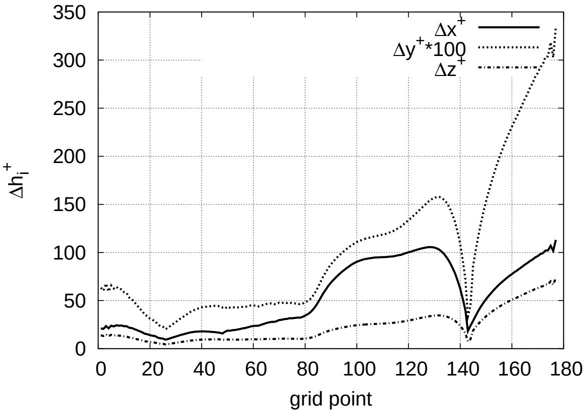

Figure 2: Near-wall resolution in terms of the non-dimensional inner coordinates Δh^+ versus grid points.

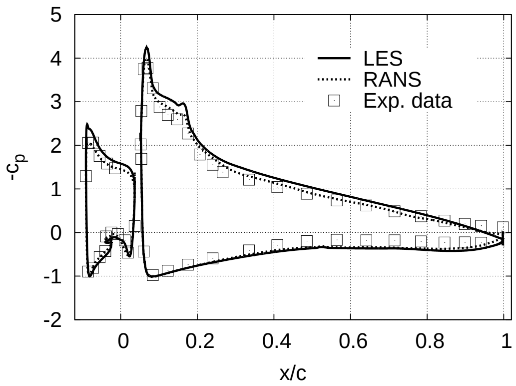

Figure 3: Pressure coefficient c_p versus c/x for LES, RANS, and measurements (Kolb 2006).

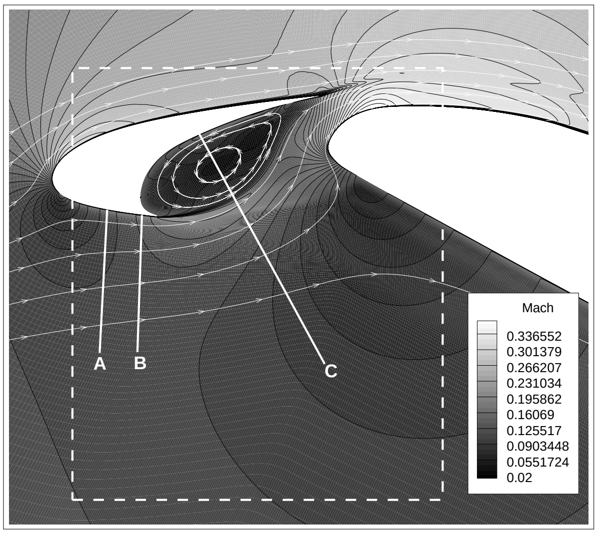

Figure 4: Streamlines and Mach number contours of the time and spanwise averaged LES flow field data. The dashed box marks the section shown in Fig. 5. The velocity distributions normal to the lines A, B, and C as a function of the coordinate s along this lines are shown in Figs. 6 to 8.

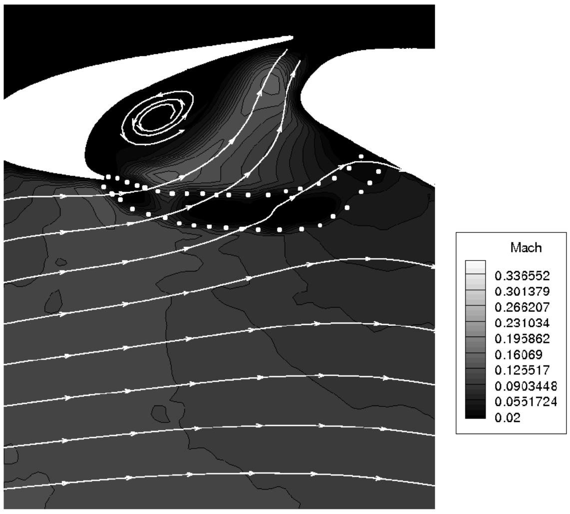

Figure 5: Streamlines and Mach number distribution of the PIV measurement. The dotted area marks the position of the slat support.

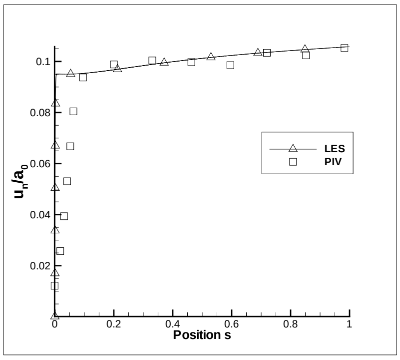

Figure 6: Distribution of the velocity on line A, which is defined in Fig. 4, as a function of the coordinate s along this line; comparison of LES and PIV data.

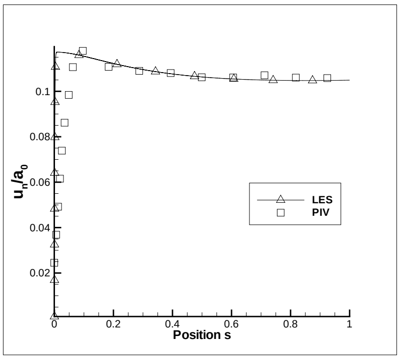

Figure 7: Distribution of the velocity on line B, which is defined in Fig. 4, as a function of the coordinate s along this line; comparison of LES and PIV data.

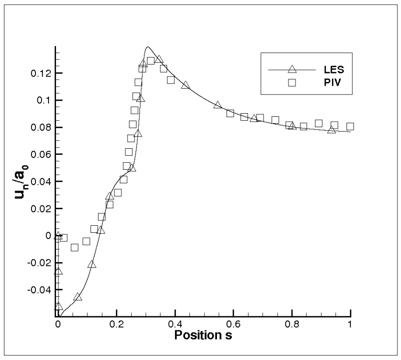

Figure 8: Distribution of the velocity on line C, which is defined in Fig. 4, as a function of the coordinate s along this line; comparison of LES and PIV data.

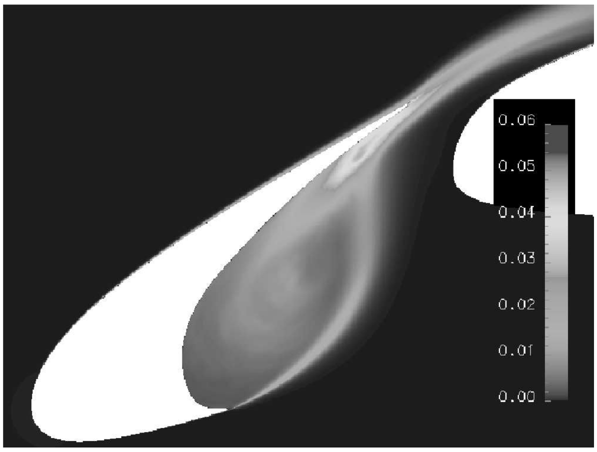

Figure 9: Turbulent kinetic energy k non-dimensionalized by u_∞^2 in the slat region .

Figure 10: Turbulent structures in the slat area visualized by λ_2 contours with mapped on Mach number distribution.

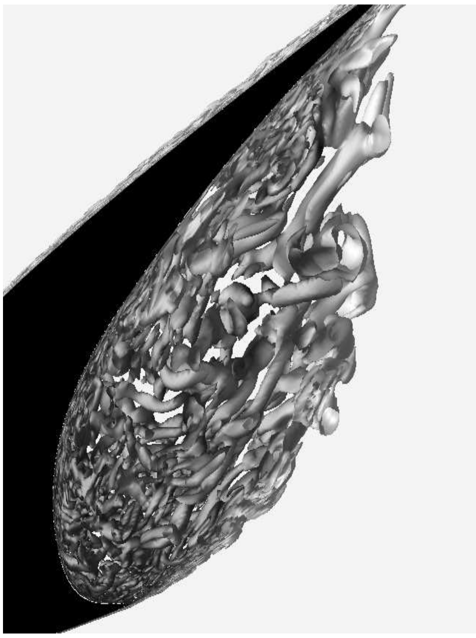

Figure 11: Vortical structures visualized by λ_2 contours in the slat cove region.

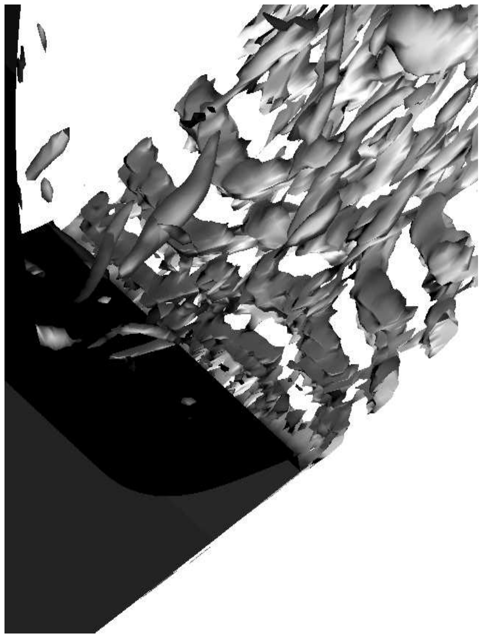

Figure 12: Development of rollers downstream of the slat cusp and penetrating vortical structures from the recirculation area visualized by λ_2 contours.

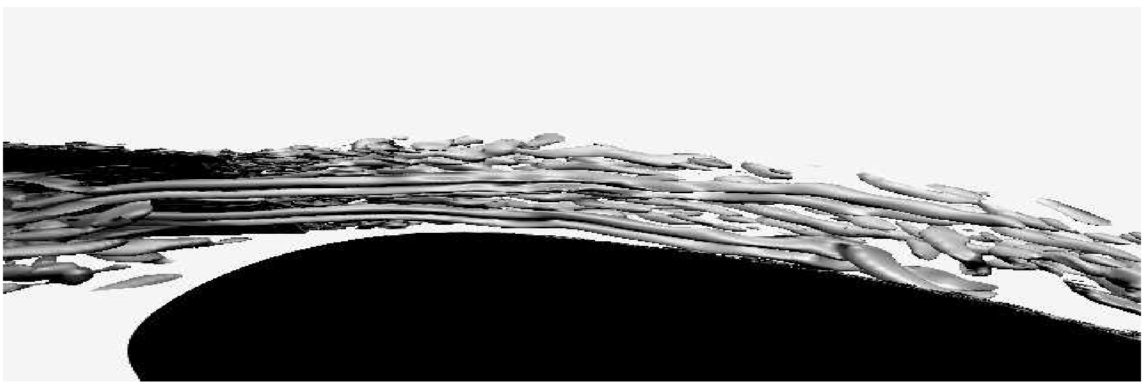

Figure 13: Wake of the trailing edge of the slat visualized by λ_2 contours; the structure is dominated by wall rips.

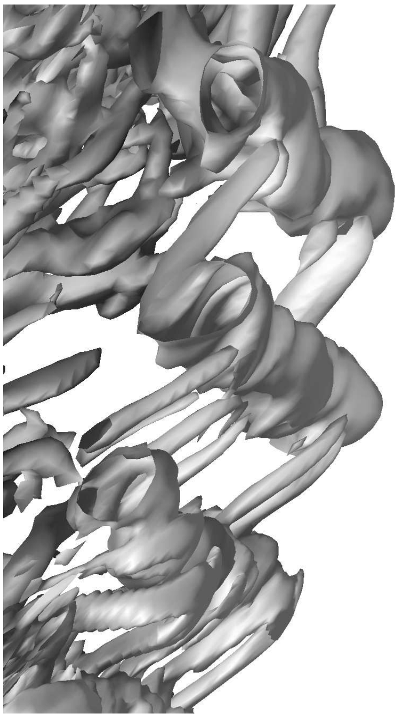

Figure 14: λ_2 contours show rollers and streamwise rib vortices in the shear layer.

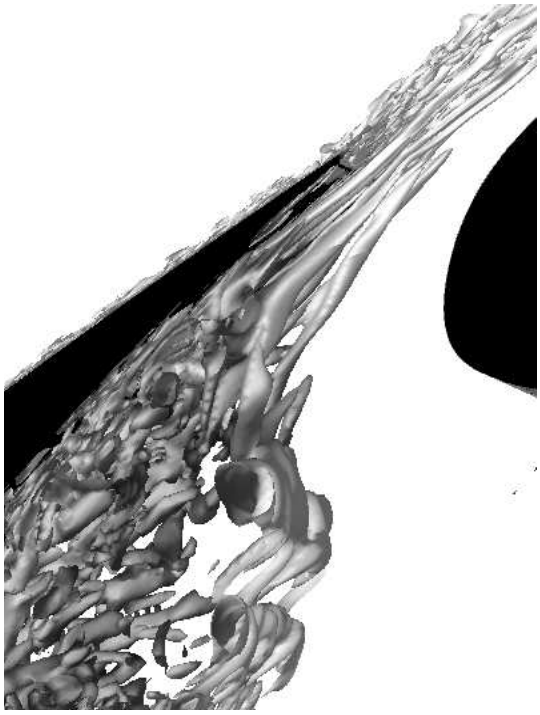

Figure 15: λ_2 contours show vortical structures in the reattachment area of the slat cove shear layer.

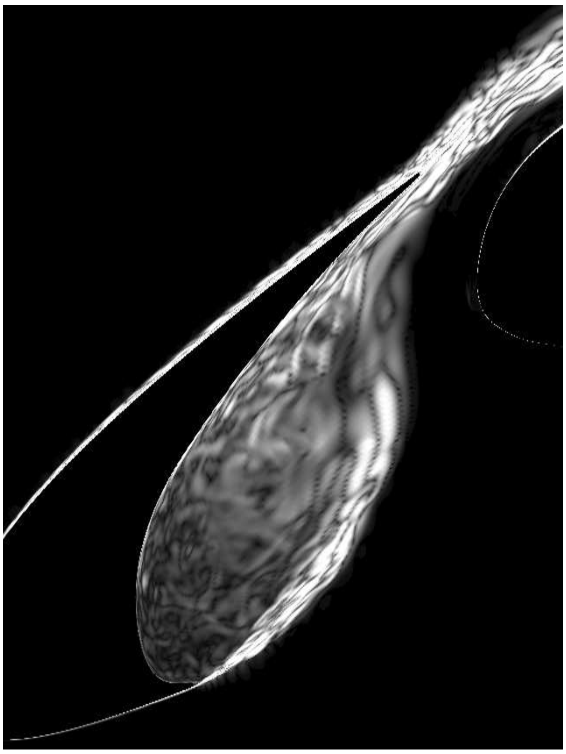

Figure 16: Snapshot of the norm of the perturbed Lamb vector in the slat region.